J Musculoskelet Neuronal Interact 2007; 7(1):9-16

2nd International Conference
on Osteoporosis and Bone Research,
October 19-23, 2005

Hylonome

Thresholding technique for accurate analysis of density and geometry in QCT, pQCT and μCT images

T.N. Hangartner

BioMedical Imaging Laboratory, Wright State University and Miami Valley Hospital, Dayton, OH, USA

Abstract

Computed tomography (CT) is widely used in the assessment of bone parameters in live patients and animals as well as bone samples. Quantitative analysis requires the segmentation of the bone from the surrounding tissue, and most segmentation methods rely on some type of thresholding technique. The aim of this communication is to highlight the influence of threshold selection on various bone parameters and recommend appropriate thresholds. Two types of information are of interest in bone analysis from images: geometric parameters and density parameters. We know from imaging theory that blurring is an inherent byproduct of all imaging methods. Depending on the threshold used for segmentation, the object boundary moves in space due to the sloping edge. It is, thus, critical to select the threshold that creates an object boundary that reflects the actual object size. Similarly, due to blurring, the imaged density shows erroneous values at the object boundaries. Such values must not be included for an accurate representation of the object density. Using a pQCT scanner and a bone phantom with known density and geometry, we show that the thresholds for geometry and density are different. The threshold for accurate geometric segmentation was 49% of the difference of the density between the adjacent tissues. The threshold for accurate density assessment was 95% of the maximum density value of the bone. These specific thresholds are valid only for the scanner tested; however, the principle for selecting the thresholds is valid across scanner platforms and scale of imaging.

Keywords: Quantitative Computed Tomography, Thresholding, Density, Area

Introduction

Computed tomography (CT) has been used for diagnostic assessment of patients for more than 30 years[1]. Soon after the introduction of CT, clinicians became interested in performing quantitative assessment of bone both in the spine[2-4] and in the forearm[5-7]. Improvement of geometric resolution led more recently to the imaging of *ex vivo* bone samples of the iliac crest[8]. Analysis of these bone images usually results in a series of parameters describing bone density of various compartments as well as bone geometry. Such descriptors require segmentation of bone from background tissue, and there are numerous methods attempting to do that. Most methods use some type of threshold criteria, possibly in combination with a gradient analysis. Depending on the amount of noise in the image and the contrast between the bone and surrounding soft tissue, such automatic procedures result in more or less successful segmentation.

Although the segmentation of bone from soft tissue is a necessary step in the analysis of most parameters, the exact position of the segmentation boundary has often not received the attention it deserves. We will consider in detail the impact of the segmentation boundary on accurate geometric as well as density evaluations from CT images.

Imaging degradation

Every imaging process degrades the information compared to the original. The degradation we are concerned about here is the blurring of edges. Such blurring can be mod-

The author has no conflict of interest.

Corresponding author: Thomas N. Hangartner, Professor of Biomedical Engineering, Medicine & Physics, BioMedical Imaging Laboratory, Wright State University and Miami Valley Hospital, 504 East Bldg., One Wyoming St., Dayton, OH 45409, USA
E-mail: thomas.hangartner@wright.edu

Accepted 31 October 2006

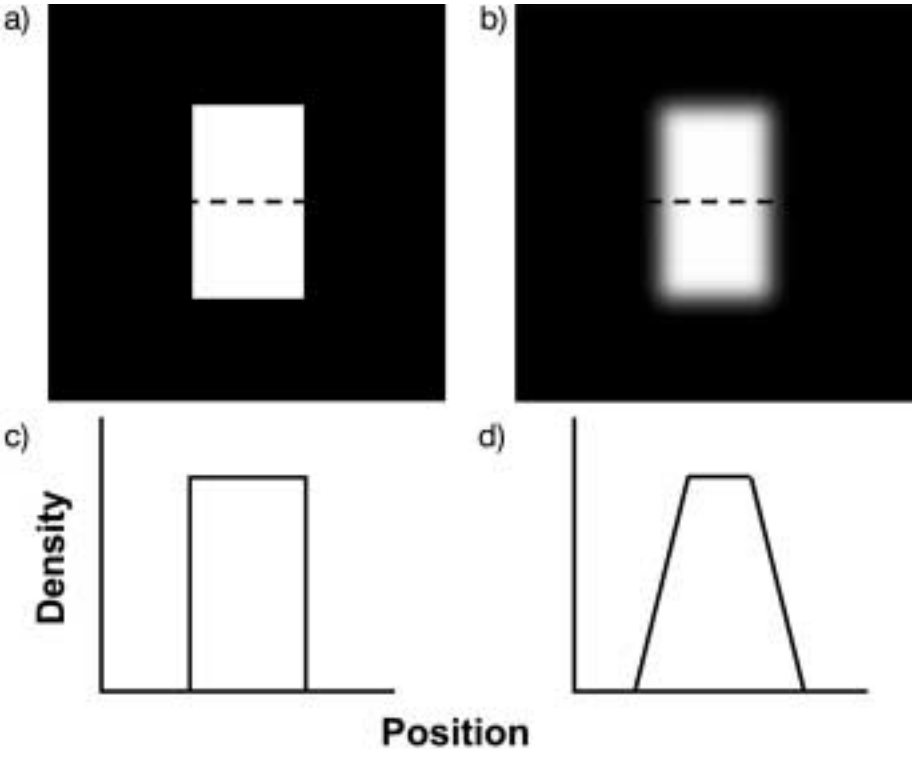

Figure 1. Simulation of blurring through imaging: a) original rectangular block to be imaged; b) imaged block with blurred edges; c) and d) profile along dashed line indicated in figure a) and b), respectively.

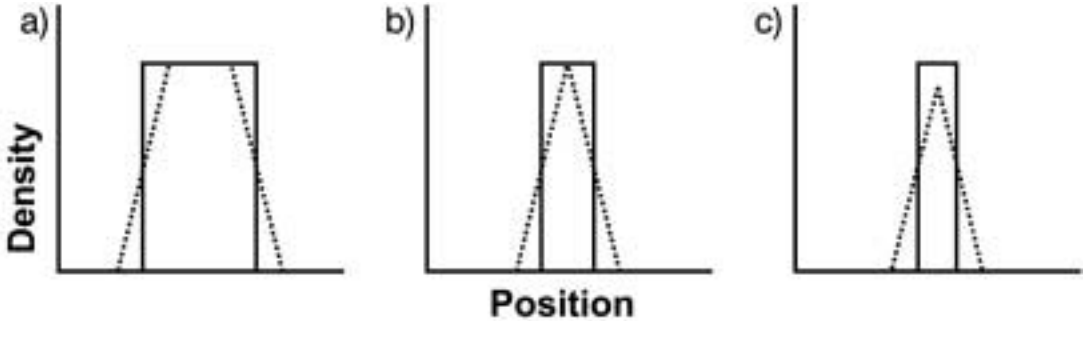

Figure 2. Profiles (dotted lines) through imaged blocks (solid lines) of gradually narrower widths (a) to c)).

eled in its simplest form as a convolution with a blurring function. For an image, the blurring function usually takes the form of a two-dimensional kernel, which is used to convolve a matrix that contains the original structure. More comprehensive analyses would require a three-dimensional matrix representation of the original structures to be imaged, which would then be convolved with a three-dimensional imaging kernel. However, for the present considerations, we will not pay attention to the third dimension, i.e. the influence of the slice thickness on image structures that are not homogenous and isotropic along the third dimension.

To simplify matters further, let us assume the image representation of a rectangular block of homogenous material. An ideal cross-sectional CT image through the block should provide an image of a rectangle with the density of the block (Figure 1a). The imaging process, represented by convolution with a Gaussian convolution kernel, will blur the edges (Figure 1b). To see in more detail the effect of the imaging process, we plot the central horizontal line through the blocks (Figure 1c, d). It is obvious that the sharp edges of the block have turned into sloping edges. In this first example, the shape of the block profile still resembles the original profile shape to some extent. If we image narrower blocks with the same imaging system, i.e. the same convolution kernel,

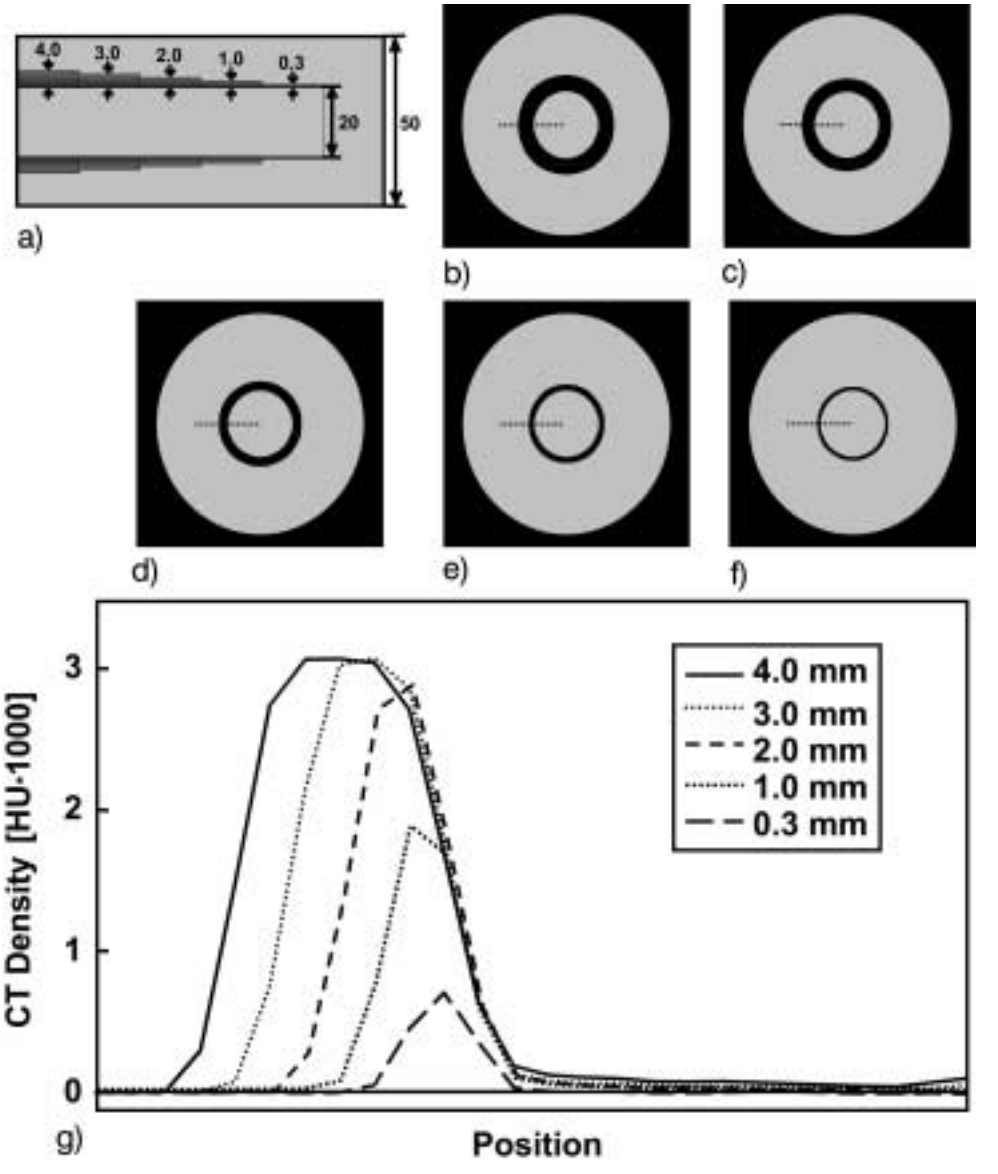

Figure 3. Measured blurred images by CT: a) cross-section through cylindrical aluminum phantom with wall thicknesses between 0.3 and 4.0 mm; all dimensions are in mm; b) to f) images through phantom at the different sections of the phantom, starting at 4.0 mm and ending at 0.3 mm wall thickness; g) line profiles through the reconstructed images along the dotted lines shown in b) to f). The y-axis represents imaged density values in Hounsfield Units (HU).

then the profiles gradually turn into the shape of a triangle (Figure 2).

We can demonstrate this behavior with CT scans of a cylindrical tube of aluminum imaged in water. The tube had wall thicknesses between 0.3 and 4.0 mm (Figure 3a) and was imaged on a peripheral quantitative CT (pQCT) scanner[9]. The images show the varying thicknesses of the aluminum walls (Figures 3b-f). Radial profiles through the walls demonstrate a similar behavior as seen with the computer simulations discussed above (Figure 3g).

There are a number of different reasons for the blurring in CT, but three of them stand out as dominant effects. The first is the finite size of the radiation beam that is used to measure the attenuation profiles necessary to generate the projections across the object. Any structure that is smaller than the beam size can not be recorded any smaller than the beam size. In addition, structures smaller than the beam size will be recorded with a reduced value proportional to their size in the beam (Figure 4). There is also a direct influence on the sharpness of an edge, which gets blurred proportionally to the size of the beam.

The second effect causing blurring stems from the reconstruction algorithm. Most algorithms in use today strike a balance between sharpness and noise in the image[10]. Thus, a

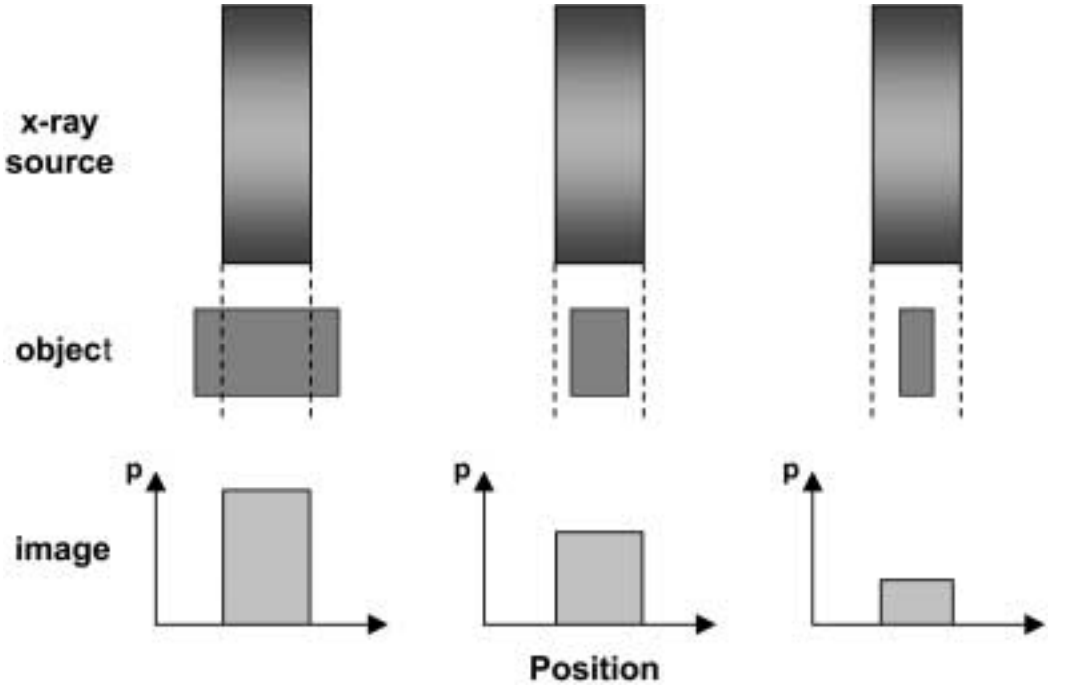

Figure 4. Illustration of recorded image values p in dependence of beam size and object size. An X-ray beam of a given size is imaging objects of gradually narrower widths (left to right). Objects that are smaller than the beam size (middle and right graphs) will not be recorded smaller than the beam size, but they will be recorded with a reduced image value.

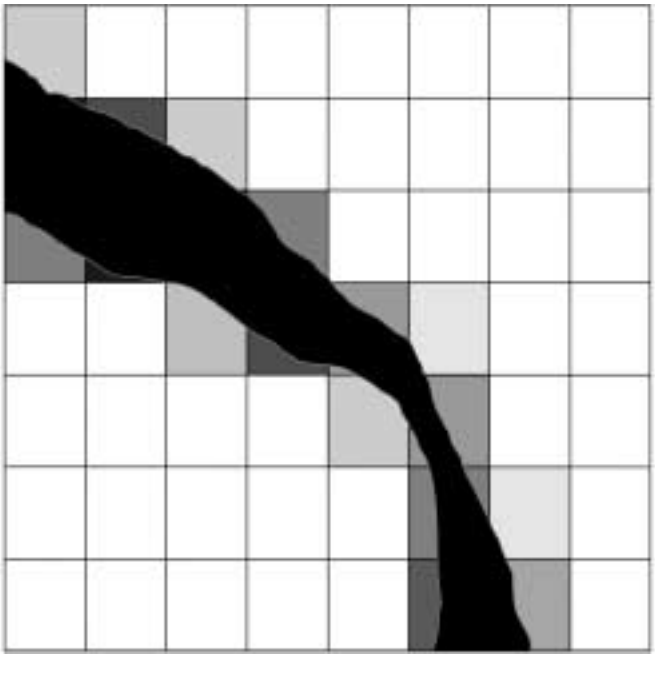

Figure 5. Illustration of blurring through finite pixel size. Bone structures that cover only part of a pixel will be represented at that location with a density value that is an average of all the densities of the various materials covering that pixel.

certain amount of blurring is induced by these reconstruction algorithms.

The third effect is based on the finite resolution of the image matrix. A given pixel can only take on a single value, and this value, if positioned at the boundary of a structure, represents the average density of all materials that cover the pixel (Figure 5). This naturally leads to additional blurring, and narrow bone structures are represented with reduced density.

Evaluation of geometry

The goal of the evaluation of bone geometry is to obtain an accurate representation of the outlines of the bone structures. Outlines are represented by thin boundary lines that are supposed to be at the exact position of the boundary of the original object. One way to obtain boundary lines for bone is by thresholding the image. Values above the threshold are considered bone; values below the threshold are considered non-bone. It is clear from Figures 1, 2 and 3 that the selection of the threshold is critical in defining an accurate boundary line. If the threshold is too low, the boundary line is too far away from the real bone boundary, and the bone structure is segmented too large. If the threshold is too high, the boundary line cuts away some of the bone, and the segmented bone structure becomes too small (Figure 6). Based on our theoretical considerations (Figure 1), the

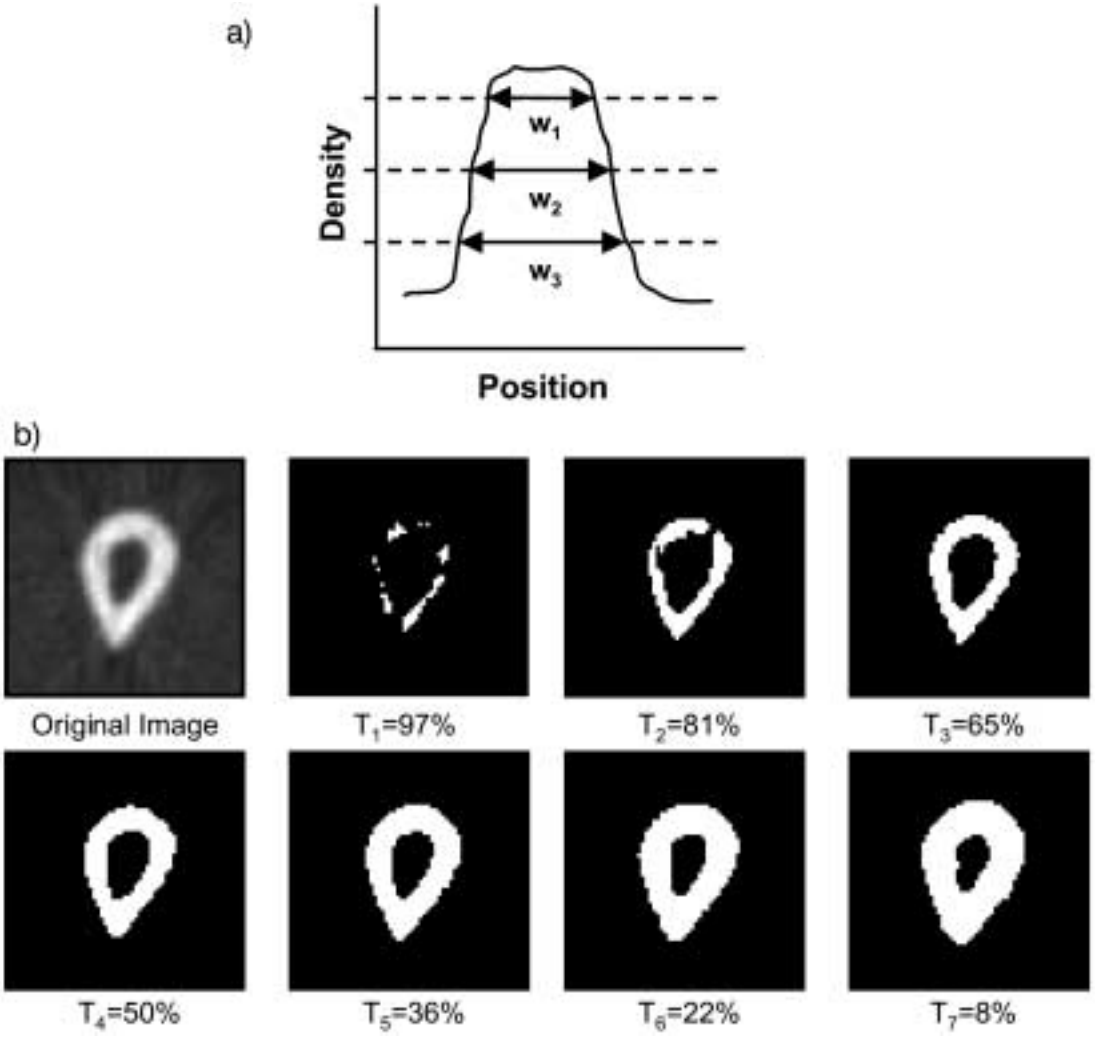

Figure 6. Influence of threshold selection on measured bone width. a) If the threshold is too high, the bone width (w_1) is underestimated; if the threshold is too low, the bone width (w_3) is overestimated. Somewhere between w_1 and w_3 is w_2, which can be obtained with the correct threshold. b) Illustration of threshold variation on a CT image of the midshaft section of a radius. The percentage values indicate the threshold levels between the densities of soft tissue and cortical bone, with 0% being that of soft tissue and 100% being that of bone.

accurate boundary of the object would be in the middle of the sloping edge curve, i.e., in the middle between the density of the bone and that of the surrounding tissue. It can be shown that the relevant upper-density parameter is the underlying density of the bone and not the imaged density of the bone[11], which is artificially reduced when the bone structure is too small (Figure 2c). For the purpose of the present communication, let us restrict ourselves to sizes of bone structures that are large enough to at least show one pixel within the bone structure with the correct value (Figure 2b).

The theoretical threshold of 50% between the materials that make up the bone boundary is only fulfilled if the imaging function has a simple form. For a specific imaging system, this threshold needs to be established experimentally by scanning an object with known geometric dimensions. If we take, as an example, the cylindrical aluminum phantom (Figure 3) with a wall thickness of 3 mm, we can extract the radial density curve and apply gradually increasing thresholds, measuring at each threshold the width of the curve. The resulting dependence of width on threshold can be plotted (Figure 7), and the threshold corresponding to the true width of 3 mm can be extracted. In this example the threshold of 1,450 HU is at 47.2% between the density of aluminum (3,073 HU) and that of water (0 HU), the two materials that make up the interface.

The most accurate results will be obtained if the materials of the phantom are similar to those of bone and the surrounding tissue. However, the threshold, as extracted with this procedure, represents a percentage value of the difference between the densities of the two materials that make up the boundary of the structure to be segmented. To obtain the

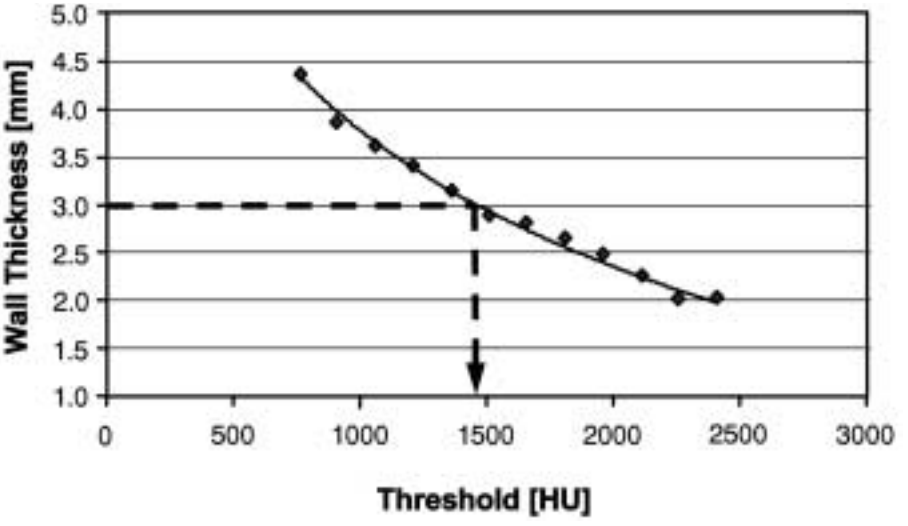

Figure 7. Calibration of threshold needed to extract the correct wall thickness of the cylindrical aluminum phantom. The width of the curve across the wall (Figure 3g) of the 3-mm-wall segment is plotted against the threshold. The threshold resulting in a wall thickness of 3 mm is assumed to be the correct threshold (arrow).

actual segmentation threshold for a given image, it is necessary to sample the density of the two materials in this image and then calculate the actual threshold at the same percentage between the densities of the two materials. For instance, if the density of the bone material is 1,100 mg/cc and that of the surrounding soft tissue is 20 mg/cc, a relative threshold of 47.2% would result in an image threshold of 530 mg/cc.

It is obvious from this calculation that the threshold depends on the density of the two boundary materials. If the interest is in segmenting the bone from the surrounding soft tissue, a single threshold will provide an accurate delineation of the periosteal boundary. In many cases, it is desirable to segment the cortex from the rest of the bone as well. So we have to establish the threshold for the endosteal boundary. Considering a cross-section through the midshaft of a long bone, we can assume, for the purpose of thresholding, that the density of marrow is sufficiently similar to that of the soft tissue adjacent to the periosteum and use the same threshold. However, if we consider a cross-section through the distal end of a long bone, the trabecular bone, which now is the material adjacent to the cortex, has a different density from that of soft tissue. This requires the calculation of a separate threshold to be applied for establishing the endocortical boundary. Without using specially developed software, the periosteal and endosteal boundaries could be extracted in two different steps and then merged to give the accurate outline of the cortex.

Evaluation of density

A common tendency is to use the segmented bone from the previous step and average the image values in the segmented region to obtain the bone density. In the case of a distal section of a long bone, where the average density in that section is the desired parameter, this approach may be reasonable. If, however, the cortex is to be evaluated, such an approach would result in an underestimation of the cortical density. From Figure 2a, it is apparent that the imaged profile within the range of the actual object boundary contains values that are lower than the flat area in the center of the curve. Averaging the density values within the segmented region is akin to averaging the values of the curve within the boundaries of the object. At both boundaries, the values are rising until they reach the flat plateau, which is the level representing the correct density. The lower values close to the boundaries are reduced due to blurring of the imaging process, also known as partial-volume effect. The error in the final density depends on the proportion of values used in the averaging process, which are suffering from partial-volume effect.

In an attempt to obtain accurate density values from CT images, it is necessary to exclude the boundary values suffering from partial-volume effect. Specialized software could perform a morphologic operation called erosion[12] to achieve this goal. In the absence of such software, the image could be thresholded appropriately to exclude the offending pixels. Because pixels suffering from partial-volume effect show a lower value than the adjacent bone pixels, an increase in the threshold will exclude most of the offending pixels. The appropriate threshold for cortical density analysis is slightly below the expected cortex value (Figure 8). We found that a threshold value of 95% of the maximum value in the cortex region produces good results.

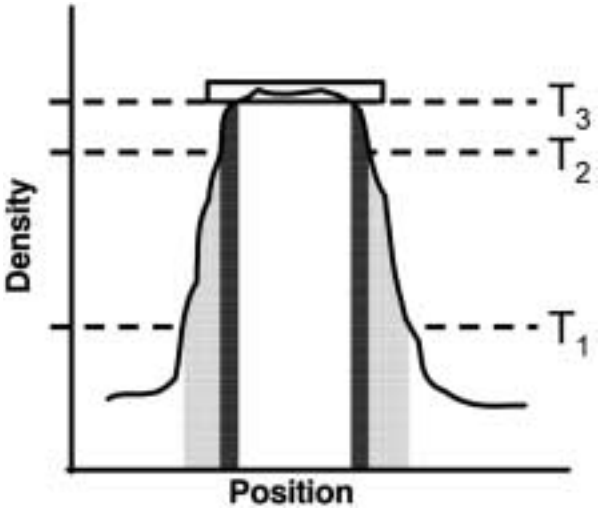

Figure 8. Thresholding for correct density value. Only the top plateau of the curve represents trustworthy density values for the measured structure; the other parts of the curve suffer from partial-volume effect. If the threshold is chosen too low (T_1 and T_2 in the illustration), then substantial regions with artificially reduced density values are part of the averaged density and produce a wrong result. Only the top threshold T_3 excludes the erroneous values.

Discussion

Imaging of bone with CT has become important *in vivo* and *in vitro*. As more research facilities use these methods, the operation of rather complex instruments is often put in the hands of laboratory personnel without specific training in imaging methods. They then rely on the manufacturer-supplied software to do the analysis. Such software, produced with the research community in mind, generally provides a large amount of flexibility in setting evaluation parameters. It is, thus, necessary for the user of modern CT equipment to understand how the choice of some of these parameters influences the data they obtain from their measurements.

We have demonstrated the appropriate choice of thresholding parameters for geometry and density, two parameters of broad interest. The issue of correct thresholding is relevant for all imaging methods. We have shown approaches on how to select the correct thresholding for CT-based images, and the approach is identical for images from whole-body, peripheral or μCT scanners. In the case of μCT, however, the density of individual trabeculae is most often not a reliably measurable parameter because the geometric resolution of most μCT systems is not adequate to resolve individual trabeculae without severe partial-volume effect (Figure 2c). However, trabecular thickness, a geometric parameter, may still be accessible with adequate accuracy.

The error of density calculations based on wrong thresholds can be substantial and depends on the ratio of boundary to area. If a large proportion of pixels is part of the boundary, the calculation of the average is more severely influenced, and the calculated bone density is more noticeably biased towards lower values. Considering a group of measurements of bones with various cortical thicknesses, the bones with the narrower cortex would show erroneously lower values. The cortical density, calculated correctly, reflects the material density of bone and would be expected to be approximately the same in normals and osteoporotics because osteoporosis does not change the composition of bone. However, in osteomalacia, osteogenesis imperfecta and other diseases where the bone composition changes, the cortex value would be expected to be different from that of normals[13].

With clinical CT scanners, it is not possible to measure the bone-material density in the trabecular region, as the limited resolution of the scanner does not allow separating out geometry and density in individual trabeculae. Thus, a reduced measured density value could be due to a reduced material density of the bone or due to a reduced size of the trabeculae. In the cortical midshaft of a long bone, however, the cortex is usually wide enough that at least some pixels in the center of the cortex are not influenced by the partial-volume effect and reach the correct density value. And these are, of course, the pixels that would be analyzed by setting the correct density threshold.

The recommended thresholding procedure for density evaluation only applies to bone structures that are wide enough such that they include some non-blurred pixels. If only blurred pixels are available (Figure 2c), then the threshold would be just below the peak, and the values above the threshold are still affected by partial-volume effect. It is, thus, necessary to investigate some radial profiles through the cortex and establish if the curve shows a plateau at the center or if the shape of the profile is more triangular, with only a single pixel showing a maximum value. Although it is possible that a single pixel reaches the correct maximum (Figure 2b), this case can not easily be separated from the case of a similar triangular profile where even the center pixel suffers from partial-volume effect (Figure 2c). It is recommended, therefore, to establish the threshold for density evaluations based only on profiles that show a clear plateau in the center.

Summary and conclusions

We have demonstrated the sensitivity of selecting the correct threshold for geometry and density analysis of CT images. We have identified procedures to establish the correct thresholds, and we have shown that two different thresholds are necessary for accurate evaluation of the most common imaging parameters: a first threshold to establish the correct geometric boundaries and a second, higher threshold to extract the correct density values from CT images.

Acknowledgement

I would like to thank Ms. Susan McGovern for editorial assistance in preparing this manuscript.

References

1. Hounsfield GN. Computerized transverse axial scanning (tomography): Part I. Description of system. Br J Radiol 1973; 46:1016-1022.
2. Cann CE, Genant HK. Precise measurement of vertebral mineral content using computed tomography. J Comput Assist Tomogr 1980; 4:493-500.
3. Laval-Jeantet AM, Cann CE, Roger B, Dallant P. A postprocessing dual energy technique for vertebral CT densitometry. J Comput Assist Tomogr 1984; 8:1164-1167.
4. Goodsitt MM, Rosenthal DJ, Reinus WR, Coumas J. Two postprocessing CT techniques for determining the composition of trabecular bone. Invest Radiol 1987; 22:209-215.
5. Rüegsegger P, Elsasser U, Anliker M, Gnehm H, Kind H, Prader A. Quantification of bone mineralization using computed tomography. Radiology 1976; 121:93-97.
6. Hangartner TN, Overton TR. Quantitative measurement of bone density using gamma-ray computed tomography. J Comput Assist Tomogr 1982; 6:1156-1162.
7. Schneider P, Borner W, Mazess RB, Barden HS. The relationship of peripheral to axial bone density. Bone Miner 1988; 4:279-287.
8. Rüegsegger P, Koller B, Müller R. A microtomographic system for the nondestructive evaluation of bone architecture. Calcif Tissue Int 1996; 58:24-29.
9. Hangartner TN. The OsteoQuant: an isotope-based CT scanner for precise measurement of bone density. J Comput Assist Tomogr 1993; 17:798-805.
10. Shepp LA, Logan BF. The Fourier reconstruction of a head section. IEEE Trans Nucl Sci 1974; NS-21:21-43.
11. Hangartner TN, Gilsanz V. Evaluation of cortical bone by computed tomography. J Bone Miner Res 1996; 11:1518-1525.
12. Serra JP. Image Analysis and Mathematical Morphology. Academic Press, London, San Diego; 1982.
13. Miller M, Hangartner T. Bone density measurements by computed tomography in osteogenesis imperfecta Type I. Osteoporos Int 1999; 9:427-432.